JOURNAL OF MATERIALS SCIENCE 13 (1978) 2119–2130

Continuous unidirectional crystallization of fibrous metasilicates from melts

A. MARIES*, P. S. ROGERS
Department of Metallurgy and Materials Science, Imperial College, London, UK

The fibrous crystalline habit observed in isothermally heated glasses of approximately metasilicate composition is due to the formation of spherulitic β-$CaSiO_3$ (wollastonite). By using the technique of hot-stage cine-micrography to measure crystallization kinetics, several 3-component systems have been selected in which growth rates are sufficiently high for the orientation of crystallization to be controlled by zone melting vitreous specimens. A development of this process has enabled β-$CaSiO_3$ filaments to be crystallized by continuous drawing from a melt contained in a resistance-heated platinum crucible, whereby the temperature of crystallization is determined primarily by the speed of drawing. X-ray and microscopic examination of these filaments has confirmed that their polycrystalline microstructure is highly oriented, with the crystallographic *b*-axis (which corresponds to the chain direction of the $[SiO_4]_3$ tetrahedra) aligned longitudinally. They possess mechanical strength and elastic modulus significantly higher than filaments of the parent glass and, as a consequence of their fibrous fracture behaviour, may be crushed into fine acicular fragments suitable for composite reinforcement.

1. Introduction

A series of previous studies in this laboratory has been concerned with the kinetics of nucleation and crystallization in glasses of approximately blast furnace slag composition, using synthetic mixtures in the $CaO–MgO–Al_2O_3–SiO_2$ system to which an addition of a transition metal oxide was made [1]. In the course of this work it was found that when the rate of internal nucleation was low, long fibrous crystals of approximately metasilicate composition were able to grow into the glass from its surface. These spherulitic crystals typically appeared as in Fig. 1, and were shown by powder X-ray analysis to consist of wollastonite ($CaO \cdot SiO_2$) in association with anorthite ($CaO \cdot Al_2O_3 \cdot 2SiO_2$). Wollastonite is the low temperature (β) polymorph of calcium metasilicate, a naturally occurring pyroxenoid often found with xonotlite ($6CaSiO_3 \cdot H_2O$) and other fibrous silicate hydrates: it is of economic value as a semi-reinforcing filler [2].

Consequently, we proposed to induce fibrous crystallization of such metasilicates in a more controlled manner by preparing glass filaments of

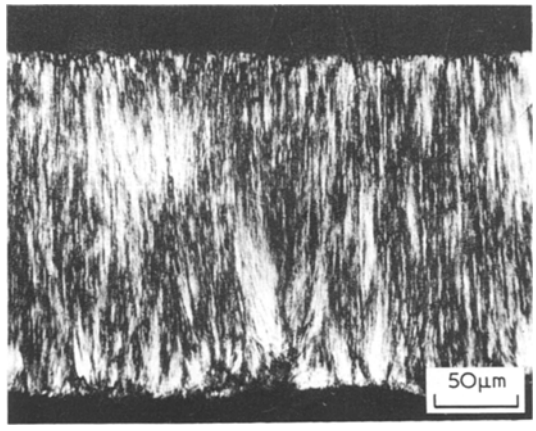

Figure 1 Optical micrograph (transmitted light, crossed polars) showing surface-nucleated fibrous crystals in a glass of composition CMASZ1 (see Table I): isothermal heat treatment at 993° C.

*Present address: ITT Components Group, Edinburgh Way, Harlow, Essex, UK.

compositions with high rates of crystal growth but little tendency to internal nucleation, and then passing them slowly through a heated zone.

2. Selection of suitable glass compositions

2.1. Glass batch preparation

Glass compositions were made up from powders: crushed pure quartz (dried at 1000° C) and analytical grade MgO and Al_2O_3 (1300° C), ZnO (900° C), and $CaCO_3$ (140° C). All powders were subsequently stored in desiccators. Each glass batch (approximately 100 g) was fused at 1400 to 1500° C for 3 h in a platinum crucible, quenched in water and crushed to a fine powder in a percussion mortar, this process being repeated twice more to ensure homogeneity.

A comparison of nominal batch composition with that obtained from analysis (by classical gravimetric methods) of some of the compositions listed in Table I shows that very little of even the more volatile ZnO was lost during glass-making. One problem which did present itself however, was corrosion of the crucible at the glass meniscus by ZnO-containing melts, particularly during the first fusion. This occurred presumably because the disproportionation equilibrium $ZnO \rightleftharpoons Zn + \frac{1}{2}O_2$ was pushed to the right in the CO_2-rich atmosphere produced by decomposing carbonates, favouring attack on the platinum by metallic zinc. ZnO was therefore added to the other batch components after CO_2 had been evolved so as to extend crucible life, but the glasses nevertheless tended to adhere strongly to the crucible.

TABLE I Batch compositions of glasses

Glass	Composition (wt%)				
	CaO	MgO	Al_2O_3	SiO_2	ZnO
CMAS1	30.00	2.00	15.00	53.00	–
CMASZ1	28.57	1.90	14.29	50.48	4.76
CMASZ3	26.09	1.74	13.04	46.09	13.04
CASZ2	36.36	–	9.09	45.45	9.09
CASZ4	36.36	–	4.55	50.00	9.09
CSZ1	35.00	–	–	50.00	15.00
CSZ2	30.00	–	–	55.00	15.00
	*30.61	–	–	54.53	14.86
CSZ3	35.00	–	–	55.00	10.00
	*35.30	–	–	54.42	10.28
CSZ4	35.00	–	–	60.00	5.00
CSZ5	40.00	–	–	45.00	15.00
CSZ6	30.00	–	–	50.00	20.00
	*29.48	–	–	50.93	19.59

*Gravimetric analysis.

2.2. Technique for measuring crystal growth kinetics

In order to be able to apply a moving zone heat treatment it was first necessary to modify the glass compositions so that rates of crystal growth would be increased by several orders of magnitude. The accuracy in measuring growth rates higher than about $1\,\mu m\,sec^{-1}$ by isothermal heat treatment of small chips of glass is inadequate because heating and quenching times become significant compared with the actual time of crystallization at the holding temperature. A method of measurement had therefore to be found which used an experimental arrangement of lower heat capacity in order to facilitate rapid changes in temperature, and an apparatus based on the hot-stage principle [3] was selected in preference to larger microfurnace designs, despite some of the drawbacks in this system which are discussed below.

A schematic diagram of our own apparatus with details of sample mounting and temperature control is shown as Fig. 2. Although hot-stage power units are available with carefully stabilized temperature control systems and electronic switching between sample heating and thermo-

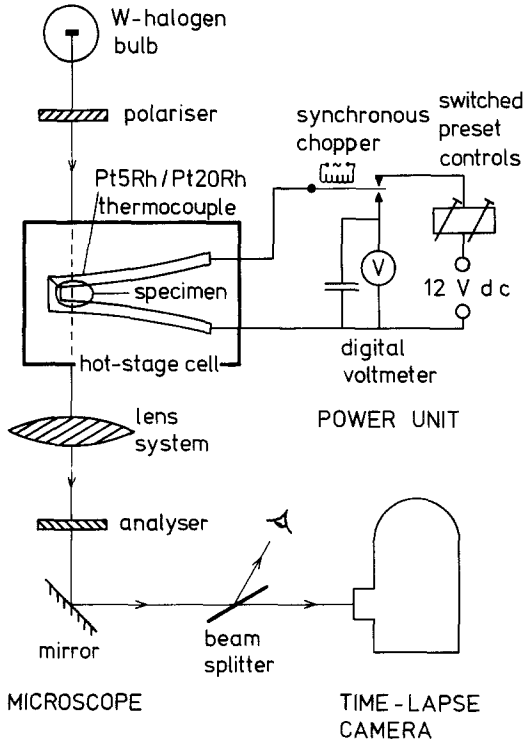

Figure 2 Schematic diagram of equipment for hot-stage time-lapse micrography.

electric e.m.f. measurement, a simpler Griffin-Telin design with a synchronous chopper operating at mains frequency was used since it could easily be adapted to switch instantaneously between preset temperatures of melting, nucleation and subsequent crystal growth, as necessitated by the highest growth rates. The Vinten "Scientific" Mk III camera could be operated in either cine or time lapse modes, but since a viewfinder could not be used during filming a beam-splitter eyepiece was incorporated in the microscope in order to observe the onset of crystallization and to focus if necessary.

Growth rate versus temperature data were obtained by sintering some of the powdered specimen on to the thermocouple and adjusting the "melt" setting on the temperature control unit so that the bead just melted. The unit was then switched to a "nucleation" setting of between 600 and 900° C for several minutes (the temperature and time depending on the glass composition) before switching to one of a range of preset "crystallization" temperatures for filming. This procedure was repeated for different temperatures of crystal growth. The 16 mm film thus generated was processed and the growth front positions were measured on a "Vanguard" motion analyser with digital output to give a sequence of coordinates on successive frames from which mean growth rates were computed. Although this technique produced apparently reliable results, they were not entirely self-consistent, and attempts were made to identify possible sources of error.

2.3. Accuracy of crystal growth-rate measurements

The crystal growth front can be followed accurately only if crystals grow in a plane vertical to the optical axis of the apparatus. With a vertical axis (as in our system) thermal convection gradients ensure that this is probably the case below the growth-rate maximum, but not so above it, where crystallization is more likely to take place along one surface of the glass bead. This explains why readings taken near the liquidus are often erratic, which is unfortunate since it is this temperature range which is most relevant to crystallization from melts. The problem can be overcome to some extent by selecting for measurement the fastest-growing crystal fronts on the film and by drawing the growth rate curve as an envelope around individual points.

The other main source of optical error is barrel distortion, which occurs because the appreciable curvature of the surface of the glass bead forms a small lens, and it is not possible to compensate for this by immersion in a liquid of suitable refractive index. Although the bead generally assumes an approximately ellipsoidal shape around an axis parallel to the thermocouple leads, crystals usually grow in a direction perpendicular to this, so that the problem reduces to one of distortion caused by spherical aberration.

An analytical expression was derived [4], by means of conventional geometric optics, for the virtual magnification M occurring at a point inside an ellipsoidal lens in terms of the dimensions and refractive index of the glass bead:

$$M = \left(1 - \frac{z}{f}\right)^{-1} \left[1 - \frac{2\rho}{f}\left\{\frac{y^2}{y^2 + (2\rho - z)^2}\right\}\right]^2 \frac{f}{\rho}\left(\frac{2\rho - z}{y}\right)^2 \quad \text{for} \quad 0 \leqslant z \leqslant \rho \tag{1}$$

(a slightly different expression holds for $\rho \leqslant z \leqslant 2\rho$) where

$$f = \left(\frac{\mu}{\mu - 1}\right)\rho \tag{2}$$

$$\rho = R_y \left[1 - \left(\frac{x}{A_x}\right)^2\right]^{1/2} \tag{3}$$

x, y and z are rectangular coordinates with respect to a fixed origin (O in Fig. 3),
A_x is the half-length of the long axis,
R_y is the half-length of the short axis,
and
μ is the refractive index of the glass.

The validity of these equations was verified experimentally, and as it was not practicable to measure all three coordinates of the crystal front as well as bead shape for every hot-stage experiment, the distortion was computed from Equation 1 for a bead of glass of representative refractive index [5] and shape for the three most probable crystal growth paths (parallel to the y-axis): on the central plane, and just inside the front and back surfaces of the bead. These calculations show that on the central plane, where most readings are taken, observed values, especially near

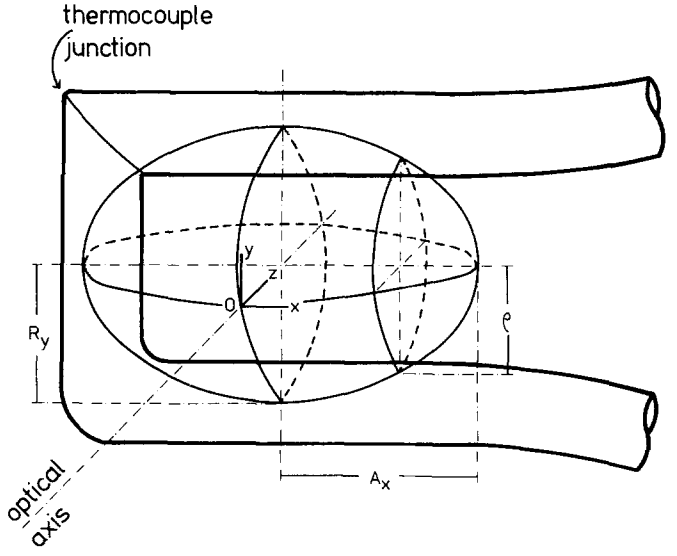

Figure 3 Geometry of hot-stage thermocouple and specimen bead.

the centre of view, are up to 30% higher than actual growth rates. Along the front surface correction factors are found to be negligible; along the back surface they rise to several hundred per cent and crystallization occurring here should not be used for measurement, though fortunately this is unlikely with a vertical optical axis.

Under most conditions of static use, the Pt 5% Rh/Pt 20% Rh thermocouple used as the hot-stage has a temperature accuracy quoted at ± a few °C. However, crystallization is a dynamic process, and liberation of the latent heat of fusion at the crystal front will raise its temperature above that of the surrounding melt. Assuming that the heat generated is lost by conduction through the melt and crystal to the thermocouple rather than by radiation to the surrounding atmosphere [6], it can be shown that the temperature difference ΔT will rise to approximately

$$\Delta T_{\max} = \left(\frac{Lw}{4\kappa}\right)U \qquad (4)$$

where

L is the heat of fusion per unit volume of $CaSiO_3$ ($2\,J\,mm^{-3}$ [7])

w is the width of the hot-stage specimen (0.4 mm)

κ is the mean thermal conductivity of melt and crystal (taken as $2\,W\,m^{-1}\,K^{-1}$)

and

U is the crystal growth rate.

ΔT will therefore rise to about 10° C at growth rates of the order of $100\,\mu m\,sec^{-1}$: temperature variations of this magnitude have been observed during hot-stage crystallization and it was consequently necessary to take averaged temperature readings.

Data from hot-stage time-lapse micrography measurements, appropriately corrected as outlined above, were used to produce the growth rate versus temperature curves shown in Fig. 4. The limited accuracy of the technique at the upper end of its range precludes its use as a means of obtaining reliable enough data to compare with a theoretical growth rate/temperature equation of the Turnbull–Cohen type, but it has proved quite satisfactory for the purposes of selecting compositions suitable for directional crystal growth experiments.

2.4. Measured crystal growth rates

The first compositions to be investigated were in the system $CaO–MgO–Al_2O_3–SiO_2$, with addition of ZnO (see Table I) since this oxide has previously been found to be a good promoter of crystal growth [8]. A search of the somewhat confused literature on viscosity in silicate systems suggested that crystallization rates might be increased by eliminating MgO and/or Al_2O_3 from these compositions, which indeed proved to be case (Figs. 4a and b).

A series of compositions was then prepared which lay within the $CaSiO_3$ primary phase region of the ternary system $CaO–SiO_2–ZnO$ and the generally high growth rates achieved in this series can be seen in Fig. 4c. Since crystallization is not an equilibrium process, not all compositions crystallized to $CaSiO_3$:CSZ5 for example, pro-

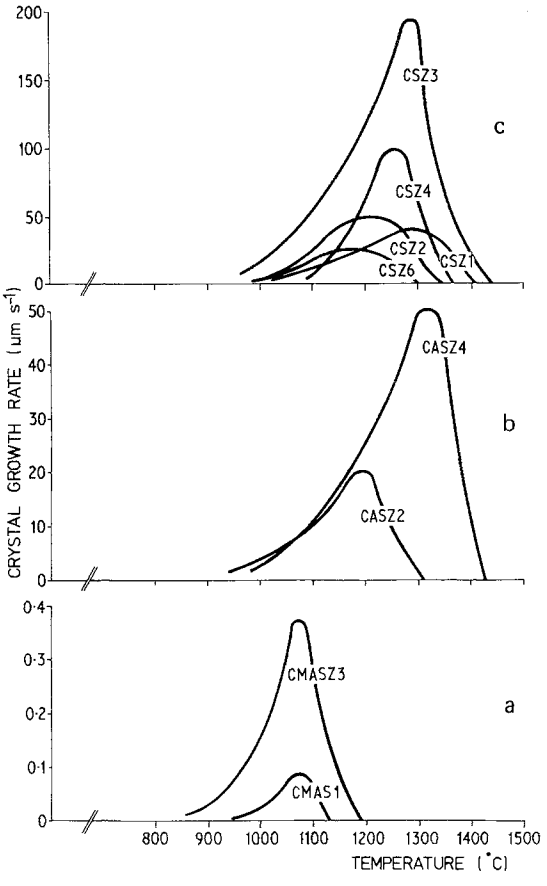

Figure 4 Crystal growth rates versus temperature determined by hot-stage micrography, in the systems (a) $CaO-MgO-Al_2O_3-SiO_2-ZnO$; (b) $CaO-Al_2O_3-SiO_2-ZnO$; (c) $CaO-SiO_2-ZnO$.

duced hardystonite ($2CaO \cdot ZnO \cdot 2SiO_2$) as well. Whether α- or β-$CaSiO_3$ crystals were grown depended on whether the temperature was above or below the $\alpha \leftrightarrow \beta$ inversion (approximately 1120° C), and also on how the crystals were nucleated: at temperatures where it was possible to grow both, α-$CaSiO_3$ crystals grew faster than β-$CaSiO_3$. In general, higher growth rates were achieved with compositions near to $CaSiO_3$ on the phase diagram [5]. This observation agrees with investigations in the $CaO-Al_2O_3-SiO_2$ system [9], where contours of maximum growth rates were found to follow closely the liquidus isotherm distribution.

3. Moving zone heating

In the first experiments, vitreous filaments 1 mm in diameter, drawn by hand from a melt supercooled to the required viscosity, were zone heat-treated in a conventional manner by passing them slowly through a sharply defined high-temperature zone produced either by thermal imaging of a tungsten–halogen lamp source [10], or by an electrically heated platinum wire coil. This did not prove to be very successful, as crystals tended to nucleate from both the interior and surface of the filament which resulted in poor alignment (Fig. 5a) and a brittle product. However, if the hot zone in the filament could be made molten its surface could not act as a source of nucleation sites, and it therefore seemed feasible to try to "zone melt" the filaments. Now whereas metals become solid immediately below their liquidus temperature, silicate melts merely increase in viscosity and it is consequently not possible to achieve a stable unsupported zone experimentally. This problem was overcome [11] by using the platinum heating coil itself as the support for the molten zone: as the filament emerged from the coil and supercooled it was in a state where its temperature was too high for internal nucleation and its virgin surface precluded external nucleation. Crystallization was initiated by introducing a platinum wire probe into the bottom of the molten zone at the start of the process, and thereafter the crystal front was self-propagating, the length of well-aligned and regularly crystalline filament that it was possible to produce being limited only by the extent of travel of the transport mechanism.

4. Crystallization of filaments drawn direct from the melt

The successful operation of this zone melting technique suggested eliminating the formation of a vitreous filament altogether, by fusing powders of appropriate batch composition to a homogeneous melt in a platinum crucible with a nozzle in its base from which filaments would then be drawn and crystallized in a continuous process. A crucible of conical shape proved to be the most suitable, because it transferred little heat to the filament emerging from the nozzle and therefore enabled a high temperature gradient to be maintained down the filament. The crucible was heated by passing currents of several hundred amperes through it via platinum arms welded to its walls which were connected to the water-cooled terminals of the secondary winding of a 25:1 step-down transformer fed through a variable auto-transformer from 240 V a.c. mains. The drawing mechanism was provided by a vernier caliper slide drawn by a cord wound round the output shaft of a suitably geared stepper motor.

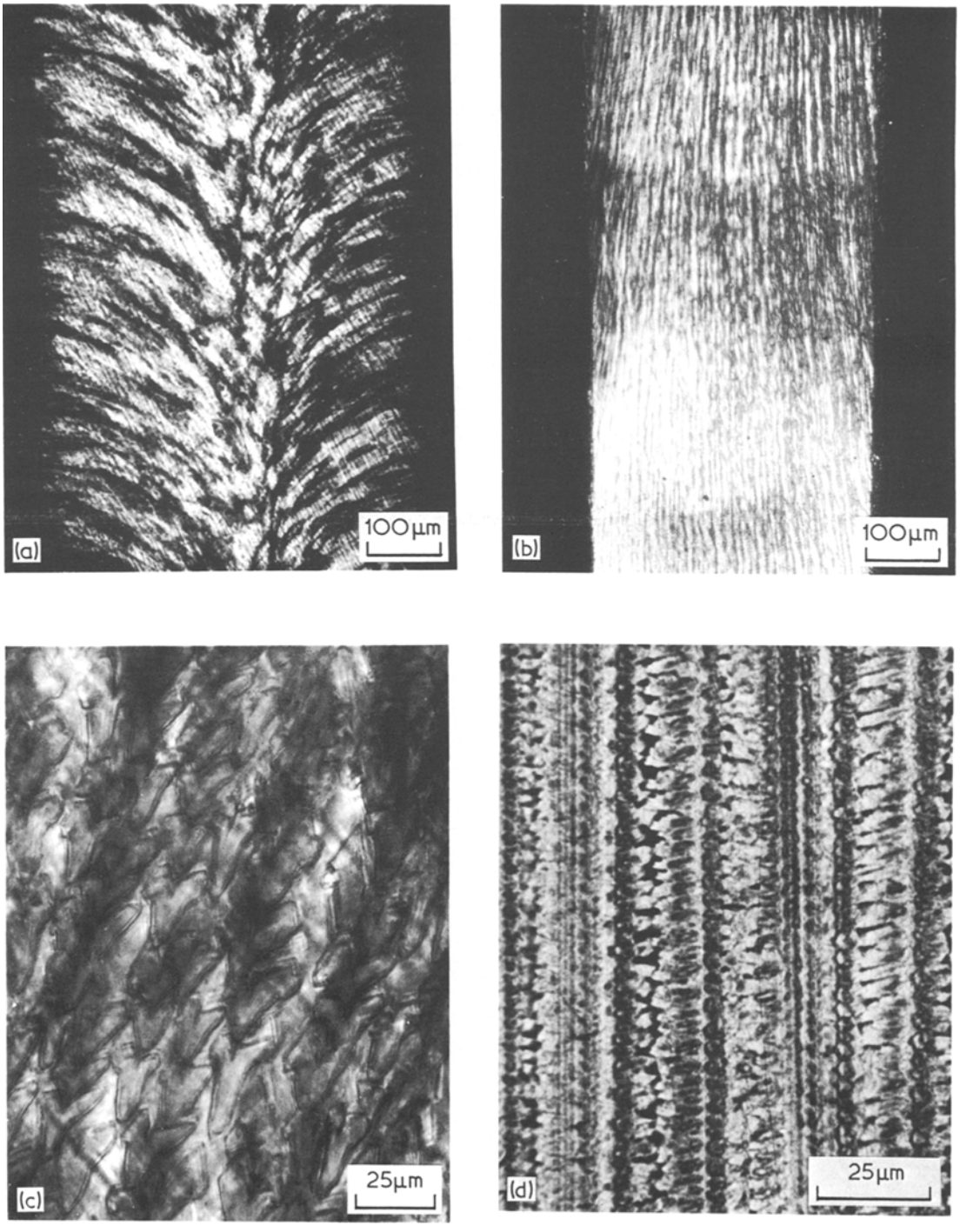

Figure 5 Optical micrographs (transmitted light, crossed polars) of crystalline filaments of composition CSZ6: (a) Glass zone-heated at 26 $\mu m\ sec^{-1}$ (β-$CaSiO_3$): longitudinal section. (b) Drawn from the melt at 38 $\mu m\ sec^{-1}$ (β-$CaSiO_3$): longitudinal section. (c) Drawn from the melt at 38 $\mu m\ sec^{-1}$ (β-$CaSiO_3$): transverse section. (d) Drawn from the melt at 7.1 $\mu m\ sec^{-1}$ (α-$CaSiO_3$): longitudinal section.

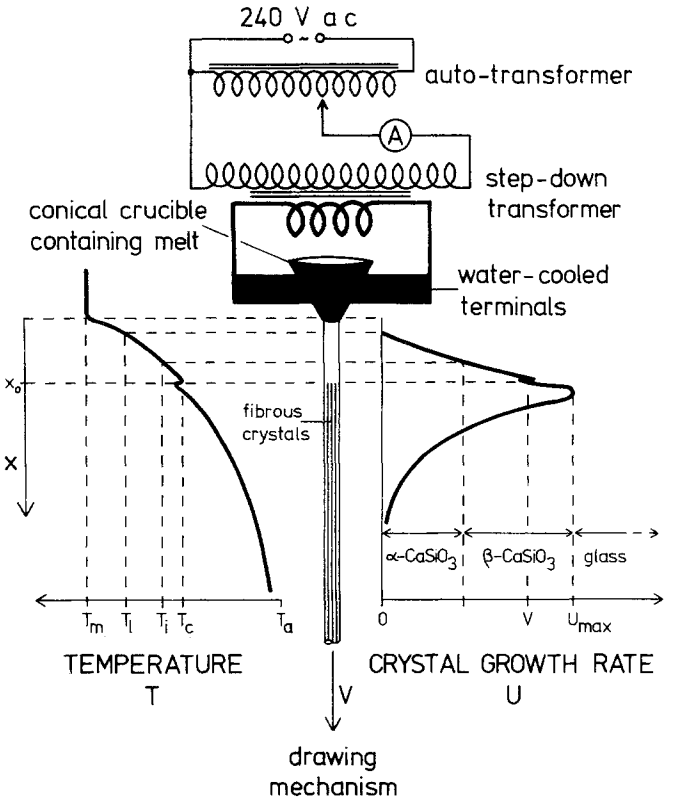

Figure 6 Schematic diagram (not to scale) of experimental arrangement for drawing crystalline filaments direct from the melt. Temperatures: T_m melt; T_l liquidus; T_i $\alpha \leftrightarrow \beta$ inversion; T_c crystallization; T_a ambient.

This apparatus proved to be very convenient to use for a much wider range of compositions than the zone melting apparatus, mainly due to the ease of varying operating parameters. For instance, by applying a cooling gas stream just underneath the nozzle, it is possible to stabilize the drawing of filaments from very fluid melts.

The experimental arrangement is illustrated schematically in Fig. 6, which also shows how the temperature profile is expected to vary down the filament (cf. Fig. 10), the discontinuity at $x = x_0$ being due to liberation of the latent heat of fusion at the growing crystal front. The vertical scale in this figure has been elongated slightly for the sake of clarity in the accompanying crystal growth-rate profile (determined by hot-stage micrography) in order to illustrate the main features of the process.

The crystal front remains stationary at a constant distance from the nozzle where the interface temperature is such that its growth rate U exactly balances the rate of drawing V: i.e. its velocity relative to the nozzle

$$\frac{dx}{dt} = V - U = 0. \tag{5}$$

In order for the crystal growth front to be stable it is also necessary that perturbations in this relative velocity should be self-correcting, i.e. that

$$\frac{d}{dx}\left(\frac{dx}{dt}\right) < 0 \tag{6}$$

or, from Equation 5, since V is constant, that

$$-\frac{dU}{dx} < 0. \tag{7}$$

The crystal growth rate profile has this required positive value for dU/dx only on the part above the maximum.

For a composition such as CSZ6, the $\alpha \leftrightarrow \beta$-$CaSiO_3$ inversion temperature intersects this part of the profile at a speed of about half the maximum growth rate U_{max}. At filament drawing speeds less than this the high-temperature polymorph α-$CaSiO_3$ will crystallize, whereas at greater speeds β-$CaSiO_3$ will crystallize. If the drawing speed exceeds the growth rate maximum however, crystallization is unable to keep pace with it, and a glassy filament is produced: it is thus possible to produce three different types of

filament from identical compositions merely by changing the drawing speed.

5. Characterization of polycrystalline filaments

5.1. Microstructural morphology

A typical longitudinal thin section of fibrous β-$CaSiO_3$, crystallized from composition CSZ6, is shown as Fig. 5b: the crystal growth habit is predominantly spherulitic in appearance. Transverse sections show that there is, in additional to the longitudinal alignment, some orientation in the plane perpendicular to this direction (Fig. 5c). Sections of α-$CaSiO_3$ reveal dendritic morphology and may also be distinguished from β-$CaSiO_3$ by their considerably higher bi-refringence (Fig. 5d). A modal analysis of these sections, carried out with a "Swift" automatic point counting stage under polarized light and observing the conditions necessary for materials with marked preferred orientation [12], showed that the volume fraction of crystals was $74 \pm 3\%$ in the β-$CaSiO_3$ and $67 \pm 6\%$ in the α-$CaSiO_3$ material, the residual phase being glass.

The scale of the fibrous microstructure varies with the rate (and therefore the temperature) of crystal growth. For β-$CaSiO_3$ the fibrils were found to become finer as the growth rate increased, while for α-$CaSiO_3$ the opposite trend was obtained. These observations may be explained in terms of current theories of crystal growth morphologies in silicate melts [13]. Spherulitic growth is likely to occur if there is a sufficient degree of reordering during crystallization for the reduced entropy change $\Delta\Sigma (= \Delta S_f/R)$ to be greater than about 4 [14]. At the melting point of $CaSiO_3$ $\Delta\Sigma = 5.5$, and at the transition temperature $\Delta\Sigma_\beta - \Delta\Sigma_\alpha = 0.4$ [7] because of the greater reordering to form the $[SiO_4]_3$ chain structure of β-$CaSiO_3$ (Fig. 7) than the Si_3O_9 rings of α-$CaSiO_3$. The high melt viscosities at undercoolings large enough to form β-$CaSiO_3$ also favour spherulitic crystal growth.

The observed dendritic crystallization of α-$CaSiO_3$ melts of relatively low viscosity correlates with this theory: it appears "fibrous" because geometric restrictions inhibit "transcrystallization" (the growth of 2° and 3° dendritic arms). The coarsening of microstructure with increased growth rates and undercoolings expected with dendritic crystallization has also been observed experimentally in α-$CaSiO_3$ filaments. β-$CaSiO_3$, on the other hand, crystallizes from more viscous melts below the $\alpha \leftrightarrow \beta$ inversion temperature in a spherulitic manner. Fibril diameters would be expected to be of the order of the impurity build-up layer width, approximating to the term diffusion coefficient (D)/growth rate (U) [15], which has values in the micron range for these melts. Such diameters have indeed been observed, decreasing with temperature according to theory. Non-crystallographic low-angle branching, seen frequently in micrographs, occurs when fibrils momentarily become wider than the steady state width D/U and split in two.

5.2. X-ray analysis

The phase composition of specimens produced by drawing filaments from the melt was determined by X-ray analysis of powder samples in a Guinier camera. In addition, the orientation of crystals within the filaments was studied by means of pinhole (Laue) X-ray transmission, using a Ni-filtered CuKα source. A small splinter (close to the optimum specimen size for metasilicate compositions, calculated from mass absorption coefficients to be about 0.1 mm thick) fractured from a filament was mounted axially on a motor spindle rotating at 1 r.p.m. in the path of the X-ray beam 25 mm from a collimator of circular aperture 0.5 mm. Plate film was positioned 50 mm from the

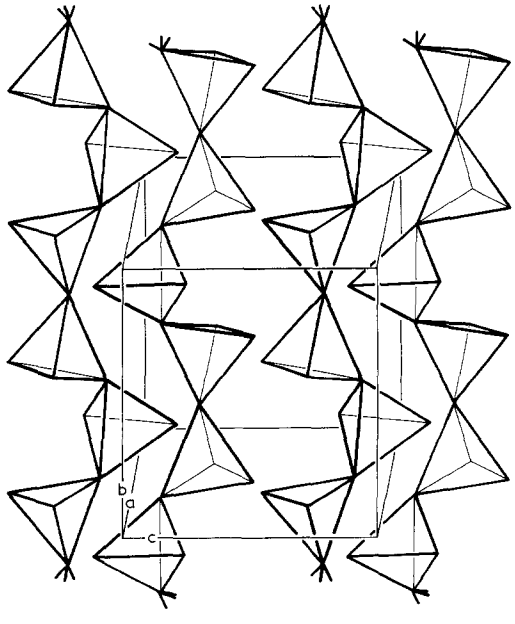

Figure 7 Projection of β-$CaSiO_3$ structure on (1 0 0), showing $[SiO_4]_3$ chains: fibre axis vertical.

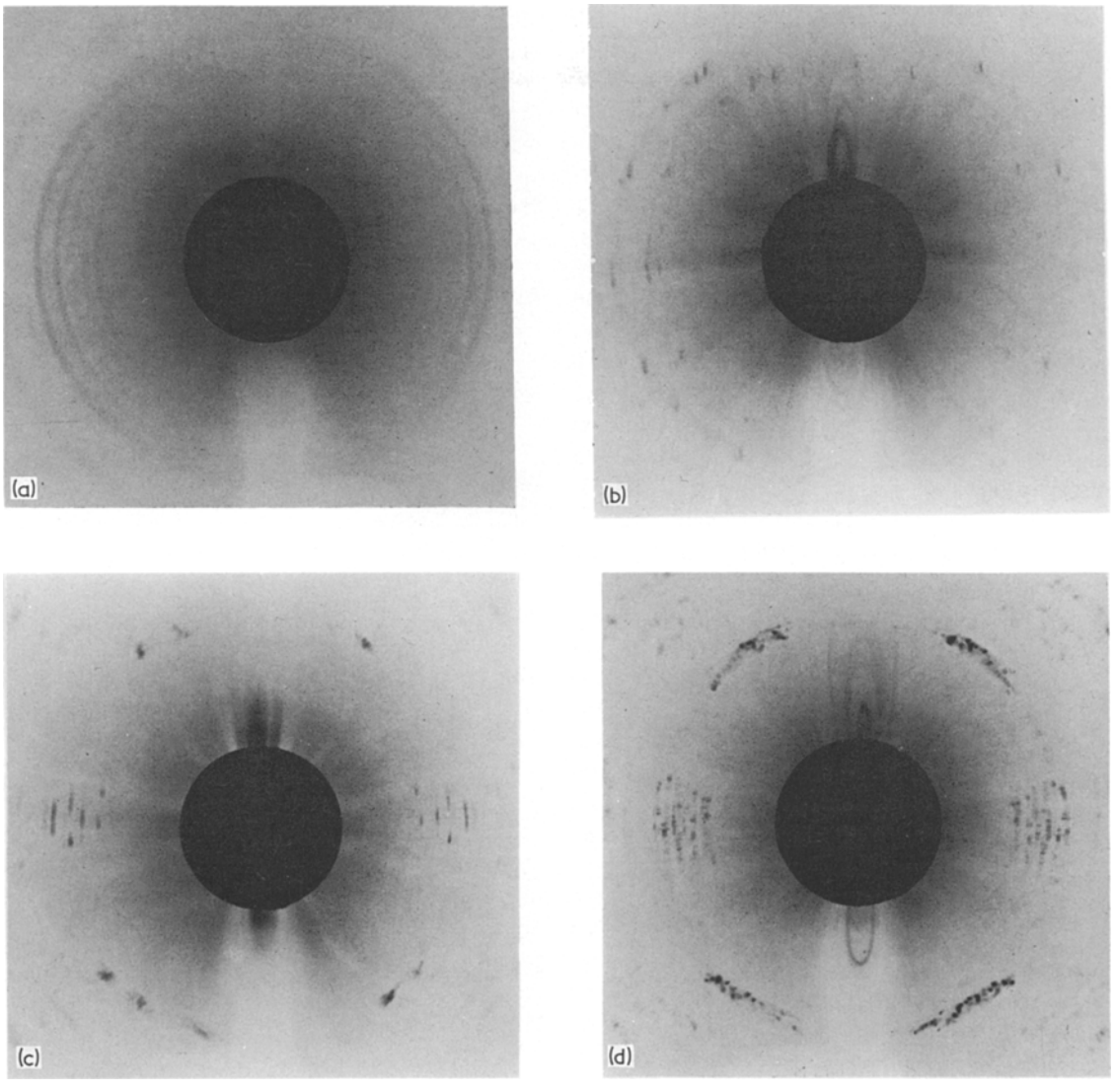

Figure 8 Laue X-ray patterns: flat plate, CuKα radiation: fibre axis vertical. (a) β-$CaSiO_3$: CSZ6 glass filament zone heated at 26 $\mu m\,sec^{-1}$. (b) α-$CaSiO_3$: filament drawn from CSZ6 melt at 7.1 $\mu m\,sec^{-1}$. (c) β-$CaSiO_3$: filament drawn from CSZ6 melt at 38 $\mu m\,sec^{-1}$. (d) Natural wollastonite from Meldon, Devon (BM 1913, 253).

specimen and exposed for 2 h to produce the diffraction patterns shown as Fig. 8.

The rings of diffraction in the pattern for conventionally zone-heated β-$CaSiO_3$ imply that the microstructure is quite randomly oriented whereas the short arcs in the patterns for α- and for β-$CaSiO_3$ drawn from the melt indicate a very high degree of orientation. Crystallite alignment in the synthetic β-$CaSiO_3$ is better than in the sample of natural wollastonite, and the crystallographic b-axis must be aligned longitudinally (Fig. 7) since nearly all the strong reflections in the pattern are $h\,0\,l$ and equatorial. The exception is the strongest, a 3 2 0 reflection with a d-spacing of 2.97 Å lying at a semi-vertical angle on the film of $33.0 \pm 0.5^\circ$, which signifies an axial unit cell dimension [16] of 7.33 ± 0.04 Å. Values of b quoted in the literature range between 7.27 and 7.32 Å [17].

5.3. Mechanical properties

The minimum specimen cross-section width for a standard test for mechanical strength in glass-ceramics such as ASTM C 158 is about 10 mm. Modulus of rupture measurements were therefore carried out on CSZ6 base glass, α- and β-$CaSiO_3$,

using commercial "Vitreosil" and "Pyrex" filaments for comparison. A specimen of about 30 mm in length was positioned in a stainless steel 3-point loading jig with a half-span of 7.5 mm between fixed 4 mm diameter rollers lined with "Teflon" tape, which was loaded in a Instron machine at a cross-head strain speed of 0.1 mm min^{-1}. As filaments were generally non-circular, the modulus of rupture and elastic modulus in flexure were calculated [18] on the basis of an elliptical cross-section at the point of fracture.

The results of the tests are shown in Table II. σ and E values for the specimens of "Pyrex" and "Vitreosil" are in reasonable agreement with data supplied by the respective manufacturers: note that the high strength of the "Pyrex" filaments is probably due to their smaller diameter. The CSZ6 base glass has a relatively high elastic modulus for a silicate, because of the "tightening" effect on the oxide lattice of the Zn^{2+} ions [19]. α-$CaSiO_3$ filaments are similar in both strength and elasticity to the base glass, whereas the enhancement in the properties of β-$CaSiO_3$ filaments is considerable. Filaments of CSZ6 glass which had been conventionally zone heated were too delicate to allow bend tests to be carried out, primarily because of the surface nucleated crystallization.

A scanning electron micrograph of the surface of β-$CaSiO_3$ material fractured in flexure along the fibril direction is shown as Fig. 9. Large fracture steps have been produced as a combination of interfibrillar and transfibrillar failure, and the work of fracture, determined from controlled fracture load–deflection curves [20], is an order of magnitude higher than for dendritic α-$CaSiO_3$

TABLE II Results of comparative 3-point bend tests: coefficients of variation for 10 specimens shown in parenthesis

Specimen	Filament diameter (mm)	Modulus of rupture ($MN\,m^{-2}$)	Elastic modulus ($GN\,m^{-2}$)
"Vitreosil" (Thermal Syndicate Ltd.)	0.92	190 (11)	65 (9)
"Pyrex" (J. A. Jobling Ltd.)	0.60	420 (25)	74 (5)
CSZ6 glass (Table I)	0.82	310 (18)	93 (3)
α-$CaSiO_3$ (ex CSZ6)	1.15	320 (30)	91 (11)
β-$CaSiO_3$ (ex CSZ6)	1.03	540 (27)	124 (9)

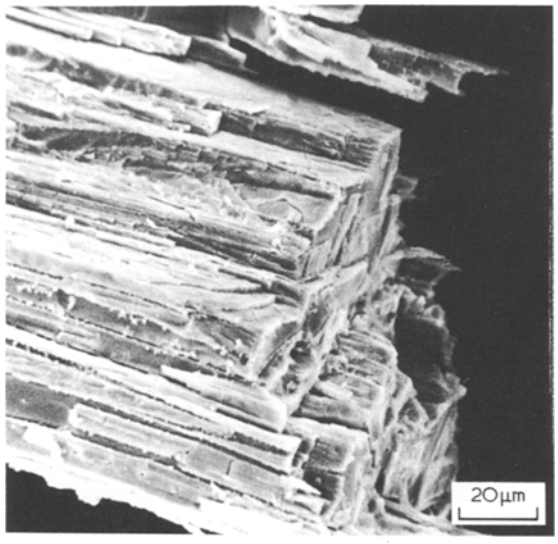

Figure 9 Scanning electron micrograph of β-$CaSiO_3$ filament crystallized from composition CSZ6 fractured in flexure (neutral axis parallel to fibril direction).

[21]. As a result of this increased degree of crack deflection, polycrystalline filaments of β-$CaSiO_3$ may easily be crushed into acicular fragments of dimensions suitable for reinforcing composite materials. Preliminary trials, consisting of application of transverse pressure to filaments between glass plates, have indicated that the highest aspect ratios are produced from compositions in which the residual glass content is low (such as CSZ3) and has also been weakened by heat treatment prior to crushing.

6. Fabrication of ceramics with oriented microstructures

6.1. Existing methods

There are principally two methods in use for making oriented polycrystalline oxide ceramics, based on eutectic solidification and on glass extrusion [22]. Near-eutectic compositions may be unidirectionally solidified either in a Bridgman-type apparatus or by slow cooling in an imposed temperature gradient to produce so-called *in situ* composites. The lamellar crystals are regular and well-aligned, but as the process is essentially an equilibrium one, maximum crystal growth rates are generally quite low (a few $\mu m\,sec^{-1}$), and there are, of course, two different crystalline phases present in the product.

Glass-ceramic type rods have been formed by extruding through opposed dies compositions

in the fluor-amphibole, fluor-mica or lithium disilicate systems [23]. The products showed only partial crystal alignment and had low crystallinity, and although they could be drawn down to quite fine filaments this introduced further but randomly oriented crystallization. Crystallinity up to 85% has been achieved using a direct extrusion process [24], but crystals were still far from perfectly aligned.

6.2. Filament drawing from the melt

Not only does our novel technique permit a much wider range of compositions to be used, but crystallization speeds are faster than with eutectic solidification because of the additional influence of large thermodynamic driving forces. The polycrystalline alignment in the filament is considerably greater than that attainable in an extrusion type of process as a result of the combination of physical movement with a temperature gradient at the crystal/melt interface which is exceptionally high, as shown by the following calculation of the temperature profile down the filament.

Heat is lost from the filament mainly by radiation, and we may neglect radial temperature variation since the observed flatness of the crystal growth front indicates that this is not significant. By considering the thermal balance in an element of volume fixed in space where there is a temperature difference δT across a longitudinal distance δx, we have

Heat flow from conduction and mass transfer = Rate of heat loss by radiation

$$\left(\frac{\pi d^2}{4}\right)\kappa\frac{\delta T}{\delta x} - \left(\frac{\pi d^2}{4}\right)Vc\,\delta T = (\pi d)\epsilon T^4\delta x \quad (8)$$

where for metasilicate compositions, typically

thermal conductivity $\kappa = 2.0$ $\mathrm{W\,m^{-1}\,K^{-1}}$
specific heat capacity $c = 3.2 \times 10^6$ $\mathrm{J\,m^{-3}\,K^{-1}}$
emissivity $\epsilon = 5.1 \times 10^{-8}$ $\mathrm{W\,m^{-2}\,K^{-4}}$.

Thus for a filament of diameter d, drawn at rate V, in the limit

$$\frac{\mathrm{d}^2T}{\mathrm{d}x^2} = \frac{T^4}{d}\left(\frac{4\epsilon}{\kappa}\right) + V\frac{\mathrm{d}T}{\mathrm{d}x}\left(\frac{c}{\kappa}\right). \quad (9)$$

There is no simple analytical solution to this nonlinear second order equation, but the accurate numerical solutions shown in Fig. 10 were obtained by using Merson's iterative method, having reformulated the differential coefficients in Equation 9 with respect to T in order to get two fixed bounds of integration [25]. These curves show that the approximate analytical solution (obtained by putting $V = 0$ and ambient temperature $T_a = 0$)

$$T = \left[x\left(\frac{18\epsilon}{5\kappa d}\right)^{1/2} + T_m^{-3/2}\right]^{-2/3} \quad (10)$$

where T is the temperature at a distance x from the nozzle which is at a temperature T_m, gives a reasonably accurate temperature profile in the region of the crystal front for most drawing speeds. It is also apparent that the temperature at which the melt is maintained (T_m) affects only the distance of the crystal growth front from the nozzle, and not the temperature gradient which, for a given thermal environment, is determined by the filament (and therefore nozzle) diameter, approximately as

$$\frac{\mathrm{d}T}{\mathrm{d}x} = -\left[\frac{8\epsilon}{5\kappa d}T^5\right]^{1/2} \quad (11)$$

When this diameter is of the order of 1 mm temperature gradients of several hundred $^\circ\mathrm{C\,mm^{-1}}$ exist at the crystal growth front, thus strongly favouring unidirectional and spherulitic crystallization.

The drawing speed V, whilst also affecting the temperature gradient slightly, is primarily responsible for determining the actual temperature

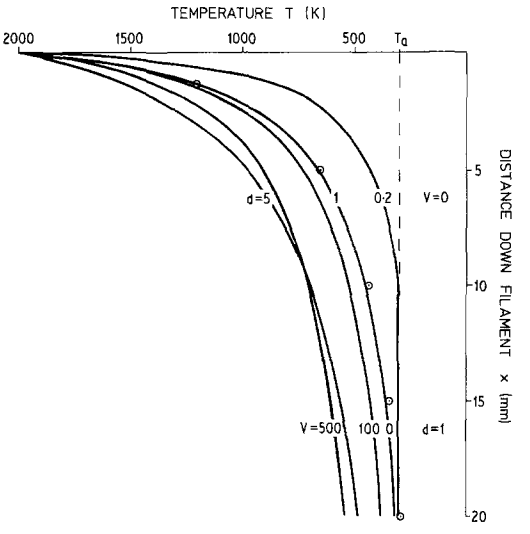

Figure 10 Longitudinal variation of temperature in filaments of diameter d (mm) drawn from the melt at speed V ($\mu\mathrm{m\,sec^{-1}}$):— numerical integration of Equation 9; ⊙ computed from Equation 10 for $d = 1$ mm.

of crystal growth, virtually independently of other process parameters. An important consequence of this is that by adjusting the melt composition so that crystallization may take place at large undercoolings, compounds which would not be formed by slow cooling of the melt (the low temperature polymorph of calcium metasilicate described in this paper being one example) may nevertheless be crystallized directly from it.

Acknowledgement

The authors thank the Science Research Council and the National Research Development Corporation for supporting this work, and are grateful to Dr R. M. Weston for helpful collaboration.

References

1. J. WILLIAMSON, *Mineral. Mag.* 37 (1970) 759.
2. R. W. ANDREWS, "Wollastonite" (HMSO, London,
3. 1970).
   J. H. WELCH, *J. Sci. Instrum.* **31** (1954) 458.
4. A. MARIES, (to be published).
5. E. R. SEGNIT, *J. Amer. Ceram. Soc.* 37 (1954) 273.
6. J. A. LAIRD and C. G. BERGERON, *ibid.* **51** (1968) 60.
7. P. J. SPENCER, *Rep. N. P. L. Div. Chem. Stand.* **21** (1973).
8. P. S. ROGERS and J. WILLIAMSON, *Verres Réfract.* **26** (1972) 53.
9. H. SCHOLZE and K.-A. KUMM, *Tonind. Ztg. Keram. Rundsch,* **93** (1969) 332, 360.
10. B. A. UNVALA and A. MARIES, *J. Phys. E* 7 (1974) 349.
11. A. MARIES and P. S. ROGERS, *Nature* **256** (1975) 401.
12. F. CHAYES, "Petrographic Modal Analysis" (Wiley, New York, 1956).
13. R. J. KIRKPATRICK, *Amer. Mineral.* **60** (1975) 798.
14. D. R. UHLMANN, "Advances in Nucleation and Crystallization in Glasses", edited by L. L. Hench and S. W. Freiman (Amer. Ceram. Soc., Columbus, 1971) p. 91.
15. H. D. KEITH and F. J. PADDEN, *J. Appl. Phys.* **34** (1963) 2409.
16. B. D. CULLITY, "Elements of X-ray Diffraction" (Addison-Wesley, Reading, 1956).
17. F. J. TROJER, *Z. Krist.* **127** (1968) 291.
18. S. TIMOSHENKO and D. H. YOUNG, "Elements of Strength of Materials" (van Nostrand, Princeton, (1968).
19. J. C. HURT and C. J. PHILLIPS, *J. Amer. Ceram. Soc.* **53** (1970) 269.
20. H. G. TATTERSALL and G. TAPPIN, *J. Mater. Sci.* **1** (1966) 296.
21. R. M. WESTON, Ph.D. Thesis, University of London (1977).
22. M. TASHIRO, T. KOKUBO, S. ITO and M. ARIOKA, *Bull. Inst. Chem. Res. Kyoto Univ.* **53** (1975) 471.
23. K. H. G. ASHBEE, *Nature* **252** (1974) 469.
24. D. I. H. ATKINSON and P. W. McMILLAN, *J. Mater. Sci.* **12** (1977) 443.
25. Numerical Algorithms Group, University of Nottingham, Document No. 502 (1972).

Received 21 November 1977 and accepted 31 January 1978.